Available online at www.sciencedirect.com
ScienceDirect
Trans. Nonferrous Met. Soc. China 32(2022) 91−103
Transactions of Nonferrous Metals Society of China
www.tnmsc.cn

Microstructure, strength and welding window of aluminum alloy−stainless steel explosive cladding with different interlayers

S. SARAVANAN[1], K. RAGHUKANDAN[2]

1. Department of Mechanical Engineering, Annamalai University, Annamalainagar, 608002, Tamilnadu, India;
2. Department of Manufacturing Engineering, Annamalai University, Annamalainagar, 608002, Tamilnadu, India

Received 16 January 2021; accepted 20 September 2021

Abstract: Aluminum 5052 (Al 5052)−stainless steel 316 (SS 316) plates were explosively cladded with Al 1100, pure copper and SS 304 interlayers. The operational parameters viz., standoff distance, explosive mass ratio (mass ratio of the explosive to the flyer plate) and inclination angle were varied and the results were presented. The advent of interlayer relocates the lower boundary of the welding window, and enhances the welding regime by 40%. A triaxial welding window, considering the influence of the third operational parameter, was developed as well. Use of interlayer transforms the continuous molten layer formed in the traditional Al 5052−SS 316 explosive clad interfaces into a smooth interface devoid or with a slender presence of intermetallic compounds. The microhardness, ram tensile and shear strengths of the interlayered clads are higher than those of the traditional explosive clads, and the maximum values are witnessed for stainless steel interlaced Al 5052−SS 316 explosive clads.

Key words: microstructure; strength; welding window; aluminum 5052; stainless steel 316; explosive cladding; interlayer

1 Introduction

Aluminum alloys are widely employed as super structure material in ship building due to their high specific strength, excellent corrosion resistance and low cost. However, the concern on the overall mechanical strength of the product is greatly mitigated by cladding with other metals/alloys [1]. Aluminum clad steel plates, fabricated by fusion welding techniques, result in the formation of undesired reaction and brittle Al/Fe intermetallic compounds [2]. The intermetallic phases, dispersed in the periphery of the interface, are susceptible to corrosion, thus, inhibiting the clad coherence. In addition, welding of Al/Fe alloys generates higher stress due to the larger variation in thermal properties such as thermal conductivity, heat capacity and thermal expansion of the participant alloys [3]. Though cladding of aluminum−steel by spot welding [4], cold roll bonding [5], diffusion bonding [6], ultrasonic welding [7], friction welding [8] and explosive cladding [9] are reported, the latter one is preferred due to the dynamic impact and short processing duration.

In an earlier attempt, ACARER and DEMIR [10] explosively cladded Al−dual phase steel under varied explosive mass conditions and reported generally straight and some wavy interfaced clads. Meanwhile, CARVALHO et al [11] analyzed the interfacial compounds formed in Al 6082−carbon steel explosive clads. Likewise, the influence of thermal kinetics in Al−steel explosive cladding was reported by SARAVANAN and RAGHUKANDAN [3]. BECKER et al [12] reported an improved fatigue lifetime for Al−steel transition joint manufactured by explosive cladding. Interestingly, HAN et al [13] observed enhanced

Corresponding author: S. SARAVANAN, E-mail: ssvcdm@gmail.com
DOI: 10.1016/S1003-6326(21)65780-1

mechanical properties while introducing a thin aluminum interlayer between the steel and aluminum plates. Recently, CHEN et al [14] have found that explosive cladding of aluminum alloy−duplex stainless steel is possible with a stainless steel interlayer. In a different approach, KUMAR et al [15] machined grooves (V and dovetail) on the base plate (SS 304) and observed the significant enhancement in the strength of the Al 6061−steel explosive clads.

In an attempt to analyze the range of explosive cladding, earlier researchers opined that biaxial welding window, between two operational parameters, is an effective approach to predict the morphology of the clad interface [16]. They generated biaxial welding windows between two operational parameters of their choice such as collision velocity−dynamic bend angle or flyer plate velocity−dynamic bend angle [17]. Of the various operational parameters, collision velocity (V_w) and dynamic bend angle (β) are of utmost importance, as they characterize the jet formation. The variation in operational parameters alters the flyer plate velocity, V_p, collision velocity, V_w and dynamic bend angle, β, and thereby different natures of interfaces viz., straight, wavy and interface with molten region, are formed [17]. Of different explosive clad interfaces, wavy interfaces are preferred due to the local work hardening of the participant alloys [18]. MOUSAVI and SARTANGI [19] reported that experimental conditions prevailing between the upper and lower boundaries of V_w−β space (welding window) result in a wavy natured interface. In this context, SHI et al [20] recommended experimental conditions closer to the lower boundary of the biaxial welding window for attaining higher strength. In another novel study, SATYANARAYAN et al [21], while joining Sn and Cu plates, extended the biaxial welding window (V_w−β) to underwater explosive cladding. Meanwhile, ÉMURLAEVA et al [22] observed coherence between biaxial welding window and numerical simulation of explosive cladding process. Though, explosive cladding of aluminum−steel plates was attempted earlier, studies on the effect of different interlayers on the microstructure, mechanical properties and positioning in biaxial welding window are limited. Hence, in this study, Al 5052−stainless steel 316 plates were explosive cladded with different interlayers and the variation in microstructure, strength of the clads and their positioning in welding window were determined and correlated with traditional explosive clads (without interlayer). In addition, the lower boundary of the welding window was constructed in a triaxial space, considering an additional operational parameter (flyer plate velocity V_p).

2 Materials, setup and calculation of explosive cladding parameters

2.1 Materials and arrangement

An inclined explosive cladding configuration with an interlayer, shown in Fig. 1, was adopted with different metallic sheets viz., pure copper, Al 1100 and stainless steel 304 interposed between Al 5052 (flyer plate: 50 mm × 100 mm × 2 mm) and SS 316 (base plate: 50 mm × 100 mm × 6 mm) plates as interlayer (size: 50 mm × 100 mm × 0.5 mm). Pure copper is a highly conductive, ductile and strong metal, while Al 1100 is a relatively weak, ductile and moderate thermal conductor. On the contrast, stainless steel 304 is an inexpensive, tough and poor thermal conductor. The chemical compositions of the participant metals (flyer, base and interlayer) are presented in Table 1.

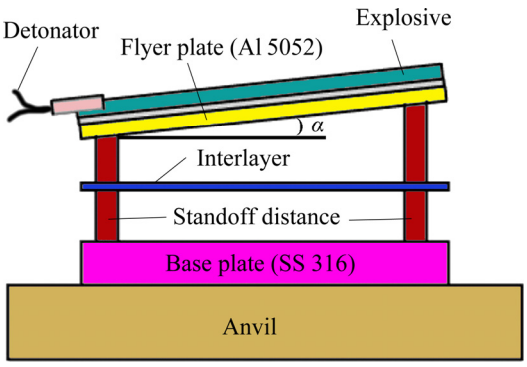

Fig. 1 Schematic diagram of interlayer explosive cladding

The initial distances between flyer−interlayer and interlayer−base plates varied between 6 and 10 mm (distance of separation, S). While the flyer plate was positioned at an angle of 6°−10° with the interlayer, a parallel arrangement was adopted between the interlayer and base plate. The chemical explosive (detonation velocity of 4000 m/s and density of 1.2 g/cm^2) was spread on the top of the flyer plate, cushioned by a buffer plate, and initiated

Table 1 Compositions of participant metals (wt.%)

Material	Cu	Mn	Si	Mg	Zn	Fe	Ti	Cr	Al	Ni	Mo	C	N	S
Al 5052	0.1	0.4	0.4	4.2	0.25	0.4	0.15	0.15	Bal.	–	–	–	–	–
Al 1100	0.0292	0.0177	0.101	0.0169	0.0158	0.479	–	–	Bal.	–	–	–	–	–
Cu	Bal.	0.0002	0.0004	0.0001	0.0004	0.003	–	–	0.001	–	–	–	–	–
SS 304	0.043	1.8	0.483	–	–	Bal.	–	18.31	–	8.44		0.015	–	–
SS 316	–	–	0.75		–	Bal.	–	11	–	14	3	.08	0.1	0.03

by an electrical detonator placed in the middle region of one end. The mass of the explosive varied such that the explosive mass ratio (mass ratio of explosive to flyer plate) varied between 0.6 and 1.0. The experimental conditions were selected based on full factorial central composite design of experiments. Sixty experiments were conducted in an explosive tank, filled with sand, and the cut sections of different interlayered explosive clads are revealed in Fig. 2. The empirical relations for different parameters of explosive cladding are given below.

Fig. 2 Photographs of Al 5052−SS 316 explosive clads with different interlayers

2.2 Calculation of explosive cladding parameters

The explosive cladding parameters after the detonation of chemical explosive are schematically illustrated in Fig. 3. The analytical estimation of flyer plate velocity, dynamic bend angle and collision velocity is given below.

The flyer plate velocity (V_{p1}) depends on the mass and detonation velocity (V_d) of the chemical explosive and calculated by [17,23]

$$V_{p1}=V_d\frac{0.612R}{2+R} \tag{1}$$

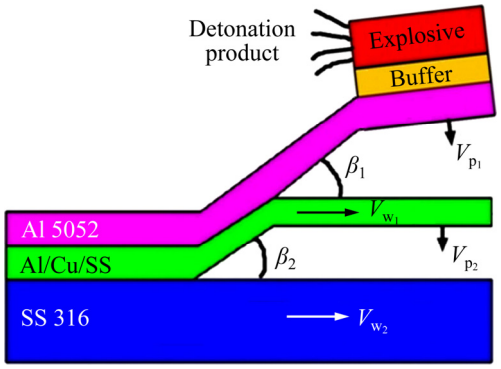

Fig. 3 Explosive cladding parameters

where R indicates the mass ratio of explosive to flyer plate. The oblique movement or the dynamic bend angle, β_1, at which the flyer plate collides with the interlayer, is mathematically estimated by [17]

$$\beta_1=2\sin^{-1}\frac{V_{p1}}{V_d} \tag{2}$$

Likewise, the velocity at which the flyer plate collides with the interlayer, i.e., collision velocity (V_{w1}), is estimated by [17]

$$V_{w1}=V_d\frac{\sin\beta}{\sin(\alpha+\beta)} \tag{3}$$

where α is the initial inclination angle between the flyer and the interlayer, and β is the dynamic bend angle. After the first collision, the flyer plate−interlayer clad moves towards the base plate (SS 316) with a dynamic bend angle (β_2) and reduced plate velocity (V_{p2}), calculated by [24]

$$V_{p2}=\frac{m_fV_{p1}}{m_f+m_i} \tag{4}$$

where m_f and m_i refer to the mass of flyer and interlayer, respectively.

2.3 Microstructure and strength analysis

Subsequent to cladding, the microanalysis samples were prepared from the central region of the clad in the direction parallel to the detonation

and were polished with various grades of emery sheets (8.4−125 μm (sieve size)) to attain 1 μm finish. Microanalysis was performed in a VERSAMET optical microscope. With respect to mechanical testing, Vickers microhardness test was conducted (ASTM E 384 standard) across the explosive clads with a load of 4.9 N and a dwell time of 15 s by a Zwick Vickers microhardness tester. Ram tensile test (Fig. 4(a): MIL−J−24445A) and side shear test (Fig. 4(b): ASTM B898—99 standard) were conducted to evaluate the mechanical properties of different interlayer-laced clads in a universal testing machine (UNITEK−94100). The average strength of three test samples for each condition is presented.

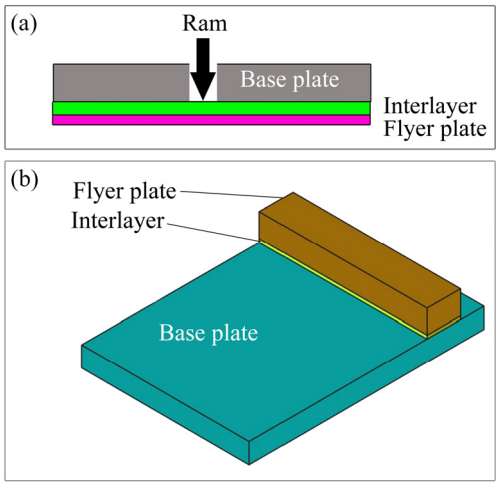

Fig. 4 Schemes of ram tensile (a) and side shear (b) tests

3 Boundaries of biaxial welding window

Biaxial welding window comprises the left, right, upper and lower boundaries which are either straight or curvy. The left boundary, a straightly natured one, denotes the minimum dynamic bend angle and collision velocity required for the characteristic wave formation. The sound velocity of the participant metals forms the right boundary of the window [17]. The curvy upper boundary defines the extreme conditions for a possible explosive clad beyond which unwarranted defects occur at the interface. The lower boundary, also curvy in nature, denotes the minimum dynamic bend angle, β, collision velocity, V_w and flyer plate velocity, V_p, required to achieve a fluid state, jetting and wavy interface [25]. The lower boundary of the welding window is analytically estimated by [17]

$$\beta = K_1\sqrt{\frac{H_V}{\rho V_{w1}^2}} \tag{5}$$

where β is in rad, K_1 is a constant (K_1=1.14), Vickers microhardness of flyer plate is denoted by H_V, and ρ represents the flyer plate density. The upper boundary of the biaxial welding window, beyond which the flyer plate damaged, is given as follows [17]

$$\sin\frac{\beta}{2} = \frac{K}{(t^{0.25}V_{w1}^2)} \tag{6}$$

where K=C_f2, C_f =$(K/\rho)^{1/2}$, K=E/[3(1−2γ)], where C_f is the compressive wave velocity, t is the flyer plate thickness, and K and E denote bulk modulus and Young's modulus of the flyer plate, respectively.

4 Results and discussion

In explosive cladding, the controlled detonation of the chemical explosive brings the aligned mating alloys at the lowest contact angle. Subsequently, the air prevailing between the participant alloys is squeezed out at the supersonic velocity as surface jetting. The jet wipes the oxide surfaces of the mating alloys, causing rapid local heating. The local heating and the stress developed by impact transform the available kinetic energy into thermal energy, which dictates the nature of interface viz., straight, wavy or interface with molten layer. The clean surfaces are compacted under high pressure from the explosion, which promotes a metallurgical bond.

4.1 Microstructure and welding window positioning for traditional cladding

The biaxial welding window for the Al 5052−SS 316 dissimilar combination, constructed using Eqs. (5) and (6) is shown in Fig. 5(b). In the biaxial welding window, dynamic bend angle (β) and collision velocity (V_w) are plotted in the ordinates and abscissa, respectively, as recommended by earlier researchers [21,22]. The lower and upper boundaries of the window are shown as curvy lines and the experimental conditions are shown as legends. It is observed that the experimental conditions are scattered closer to the lower boundary of the biaxial welding window. Further, it is observed that the dynamic bend angle is inversely proportional to the collision velocity.

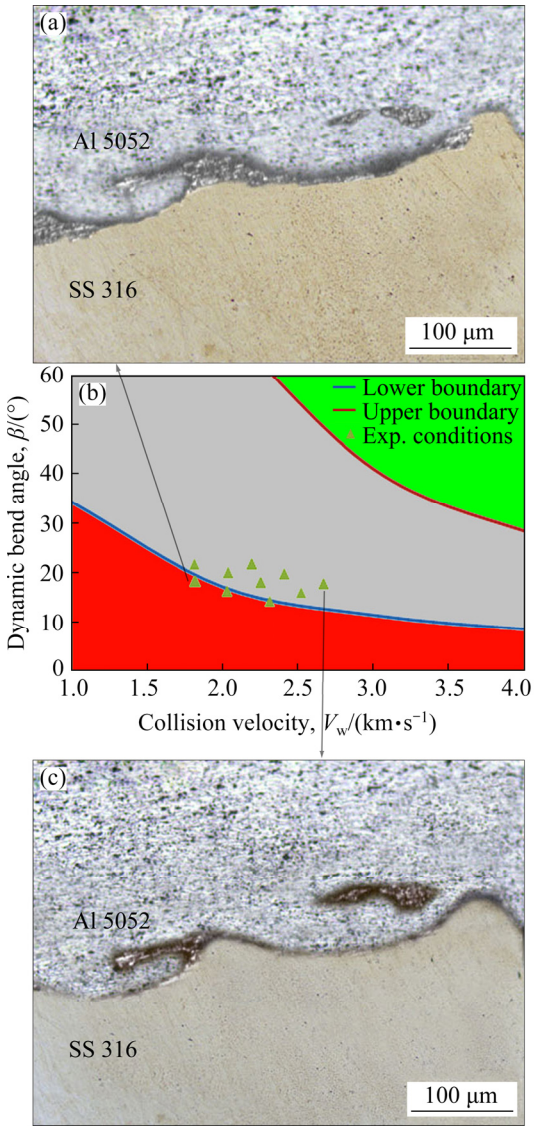

Fig. 5 Microstructures (a, c) and biaxial welding window (b) of Al 5052−SS 316 explosive clad

The interfacial microstructures Figs. 5(a) and (c) present the characteristic and interesting features associated, exclusively, with explosive cladding process. Undulating, but non-uniform, wavy interface of the flyer (Al 5052) and base plate (SS 316) is witnessed in Fig. 5(a). Vortices of the participant plates are distinct and clear, with swirls predominant, at the tips, thus indicating that the joining of the plates is by spiral morphological mechanism. This is a consequence of the fluidized behaviour of the participant plates. MAHMOOD et al [26] also observed the spiral natured interfacial mixing in their attempt of cladding titanium−copper plates.

Owing to the difference in thermal conductivity of the participant metals (Al 5052: 138 W/(m·K); SS 316: 16 W/(m·K)), the molten layer formed at the interface is entrapped and solidified. A thin, continuous layer of molten metal is formed, which is thicker at the crests and thins out in the plains. Small and isolated pockets of solidified melts are present above the waves as the metallic jets experience incomplete purge due to the rapidity of the explosive cladding process (≤50 μs). The variation in the structure of the stainless steel (BCC, up to 911 °C) and aluminum (FCC) also promotes the formation of intermetallic compounds in Al 5052−SS 316 explosive cladding. In addition, trapping of jet is seen as island inside the aluminum region.

On the other hand, Fig. 5(c) reveals a wavy morphology with a very thin, negligible, molten layer, and a vortex-free, swirl less contour. The swirls at the wavy crests are absent and a few pockets of molten layers are observed. Molten layers, i.e. the source of weakness, indicate the non-chemical equilibrium and provide the occurrence of intermetallic compounds.

Nevertheless, Figs. 5(a) and (c) are correlated with the location of the experimental points in the welding window. It is observed that the experimental conditions selected within the left corner of the lower boundary result in minimal or absence of molten layer, and experimental conditions outside the lower boundary disclose tendencies to produce a clad with intermetallic compounds. The expense of kinetic energy of the process, the results of XRD, the presence of intermetallics and the strength of the clads are discussed below.

During explosive cladding process, the dynamic impact of flyer plate with the base plate leads to shear deformation and promotes the dissipation of available kinetic energy at the interface. The kinetic energy spent ($\Delta(KE)$) at the interface is estimated by [27]

$$\Delta(KE)=\frac{m_f m_b V_{p1}^2}{2(m_f+m_b)} \tag{7}$$

where m_b indicates the mass of the base plate. The shear deformation promotes a high velocity metallic jet comprising mating surfaces that cause variation in the interfacial amplitude for the maximum (1.61 MJ/m^2, 56 μm) and minimum (0.77 MJ/m^2, 40 μm) kinetic energy conditions. The XRD analysis (Fig. 6) performed at the intermetallic

compound shows larger concentration of aluminum (weaker parent metal) as well as slender presence of Al_3Fe and $FeAl_2$ compounds, as observed in Al−Fe phase diagram and similar to the studies of SHIRAN et al [28].

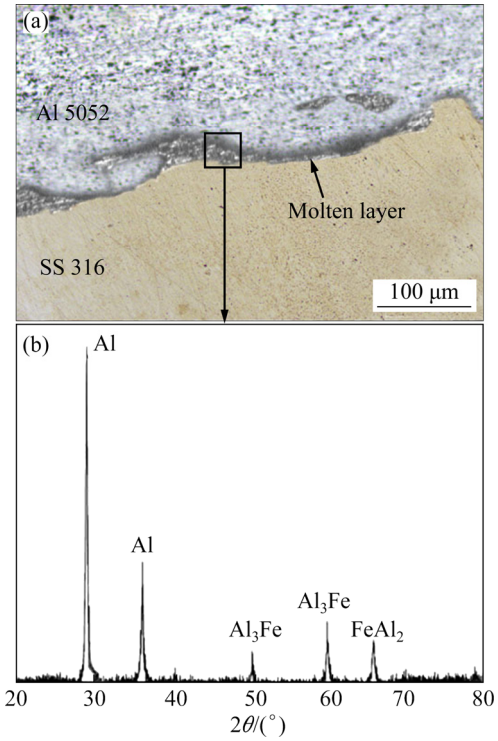

Fig. 6 Microstructure (a) and XRD pattern (b) Al 5052−SS 316 explosive clad

4.2 Effect of different interlayers on welding window and microstructure

In explosive cladding with an interlayer, earlier researchers developed separate welding windows between flyer−interlayer and interlayer−base plates, respectively. However, in this study, an attempt is made to represent both (flyer−interlayer and interlayer−base) collision conditions in a single welding window. During the initial collision (flyer−interlayer), the interlayer is considered as the base plate; whereas in the subsequent collision, the interlayer-flyer plate clad is treated as the flyer plate. The developed window provides an insight into the collision conditions in a single plot, instead of two separate plots. The judicial selection of flyer plate and interlayer properties during the plotting of welding window is a possible limitation.

The biaxial welding windows for the Al 5052−SS 316 explosive clads with different interlayers are investigated. Though the welding windows resemble the same, the positioning of the welding conditions varies with the employed interlayer. For the three different interlayers used, the welding conditions of flyer interlayer (first collision) fall between the upper and lower boundaries (shown in violet color) and are adjacent to the lower boundary; whereas the welding conditions for the second collision (interlayer−base) are located below the lower boundary (shown in red color) of the welding window. Further, the interface microstructures show a smooth wavy interface with smaller amplitude and a slender presence of molten layer. The interlayer operates as a diffusion barrier between flyer and base plates and inhibits the probable intermetallic compound formation.

4.2.1 Aluminum 1100 interlayer

The introduction of lower density aluminum 1100 interlayer (2700 kg/m^3) causes the flyer plate to initially collide with the interlayer. Subsequently, the flyer−interlayer clad travels towards the base plate, and thereby contact area of cladding, duration of collision and kinetic energy utilization are nearly doubled as stated by MANIKANDAN et al [29]. The flyer−interlayer collision (Al 5052−Al 1100) condition is located well within the lower boundary of the V_w−β space (Fig. 7(a)).

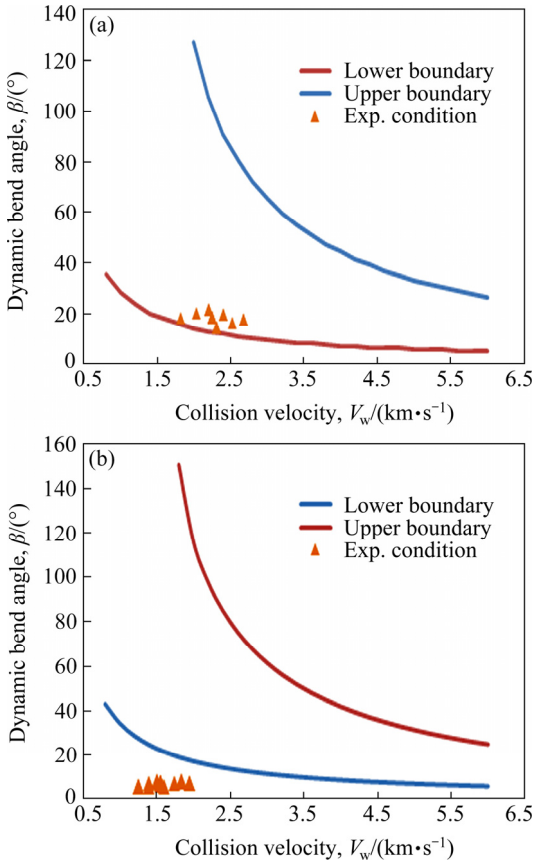

Fig. 7 Flyer−interlayer (a) and interlayer−base (b) welding windows

After the first collision, the flyer−interlayer clad faces a decline in dynamic angle and collision velocity by 50% and 15%, respectively. The reduction of operational parameters during the second collision (Al 1100−SS 316) causes the experimental conditions to be shifted beneath the lower boundary of the biaxial welding window (Fig. 7(b)). Though the second collision falls outside the welding window, successful clads are formed, indicating that the use of interlayer enhances the welding regime. The two welding windows (flyer−interlayer (Fig. 7(a)) and interlayer−base (Fig. 7(b)) are superimposed in a single welding window, and shown in Fig. 8(b).

The interface microstructures of experimental conditions, prevailing inside (flyer−interlayer) and outside (interlayer−base) the lower boundary of the biaxial welding window, exhibit a wavy and a straight interface, respectively. In addition, formation of defects such as molten layer and trapping of jet, seen in the interlayerless cladding (detailed in the previous section), is smaller. The flyer−interlayer interface in higher kinetic energy condition (Fig. 8(c): 1.86 MJ/m^2) exhibits an interfacial amplitude of 15 μm, while it declines to 8 μm for the lower energetic condition (Fig. 8(a): 0.89 MJ/m^2). However, the interface between dissimilar alloys (Al 1100−SS 316) reflects a straight interface and is in agreement with their positioning in the biaxial welding window. The reduction in interfacial amplitude is attributed to the utilization of available kinetic energy at the two interfaces. Formation of straight interface in Al−Al cladding and interface exhibiting lower amplitude in Al−steel cladding is consistent with different studies of GRIGNON et al [30] and CARVALHO et al [31], respectively. Formation of a slender continuous molten layer is witnessed at the second interface for the highest kinetic energy condition (Fig. 8(c)), as the available energy dissipation is concentrated in the region. It is inferred that, higher kinetic energy utilization promotes elevated temperature at the interface to result in the melting of participant alloys. The alloy having lower melting temperature will melt earlier than the other alloy having higher melting temperature. This is evident in the XRD pattern, as larger peaks of Al compounds are witnessed followed by Fe along with few traces of Cu (Fig. 9).

4.2.2 Stainless steel 304 interlayer

Using stainless steel 304 with higher density (7900 kg/m^3) as interlayer, three-fold denser than

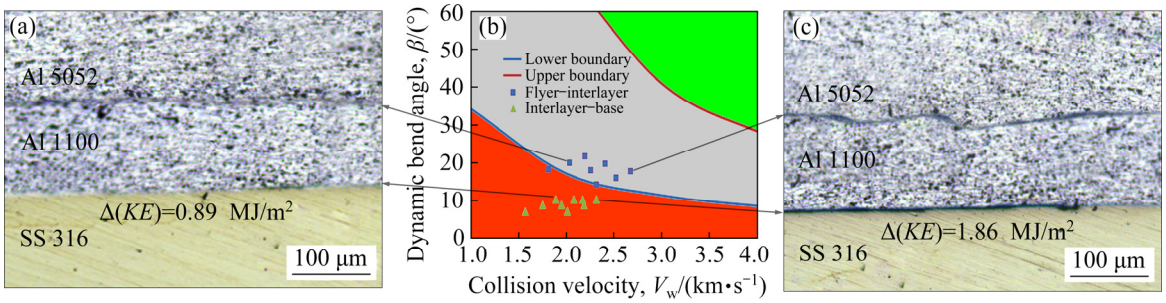

Fig. 8 Effect of Al 1100 interlayer on microstructures (a, c) and biaxial welding window (b) of Al 5052−SS 316 explosive clad

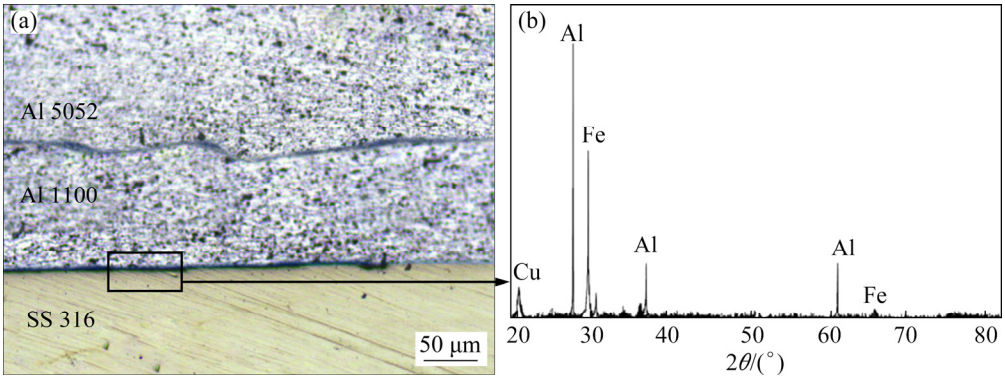

Fig. 9 Microstructure (a) and XRD pattern (b) of Al 5052−Al 1100−SS 316 explosive clad

aluminum and melting at 1385 °C, relocates the positioning in the combined biaxial welding window (Fig. 10(b)). The higher density SS 304 interlayer reduces the dynamic bend angle, β (Eq. (2)), and the collision velocity, V_w (Eq. (3)) significantly, based on the choice of process parameter values. The dynamic bend angle varies from 14.1° to 21.7° for the first collision; whereas for the second collision, it ranges from 5.67° to 8.13°. Likewise, based on the range of process parameter opted, collision velocity reduces by 14%−45%. In addition, the kinetic energy increases by two-fold than aluminum interlayered clad (Eq. (7)). The variation in the operational parameters causes the experimental conditions to be scattered inside and outside the biaxial welding window but closer to the lower boundary (Fig. 10). The experimental conditions for the collision between flyer and interlayer prevail well inside the boundaries of the biaxial welding window. However, the use of higher density stainless steel interlayer pushes the second collision condition (interlayer−base) further outside the biaxial welding window in the V_w−β plot.

The interface microstructures for the stainless steel interlayered clad display a straight profile on the dissimilar alloy interface (flyer−interlayer: Fig. 10), irrespective of the kinetic energy conditions (from 2.02 to 0.96 MJ/m^2), whereas the interface of the similar alloys exhibits undulation (25 μm) for a higher kinetic energy condition. The quantum of kinetic energy utilization for the interlayered conditions is determined by [24]

$$\Delta(KE)=\frac{m_f m_b V_{p1}^2}{2(m_f+m_b)}+\frac{M m_b V_{p2}^2}{2(M+m_b)} \quad (8)$$

where M denotes the combined mass of flyer plate and interlayer. In lower kinetic energy condition (0.96 MJ/m^2), no visible defects such as molten layer or jet trapping are formed in the two interfaces, whereas intermittent presence of molten layer is visible on the two interfaces in higher kinetic energy condition (Fig. 10(c)). The molten region at the dissimilar interface, analyzed by XRD analysis, confirms the presence of $FeAl_2$ and Al_3Fe compounds (Fig. 11).

In addition, the disparity between aluminum and steel such as poor ductility (0.3) and lower thermal conductivity (16 W/(m·K)) of stainless steel contributes to the quantum of plastic deformation and eventual formation of straight interface or molten layer formation [32]. The slender

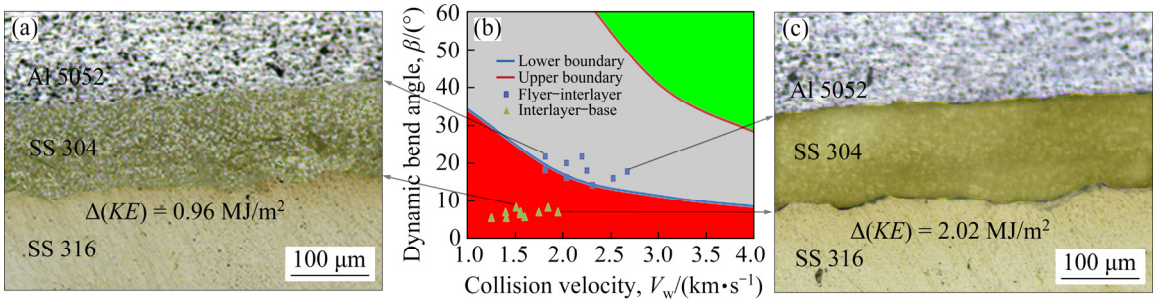

Fig. 10 Effect of SS 304 interlayer on microstructures (a, c) and biaxial welding window (b) of Al 5052−SS 316 explosive clad

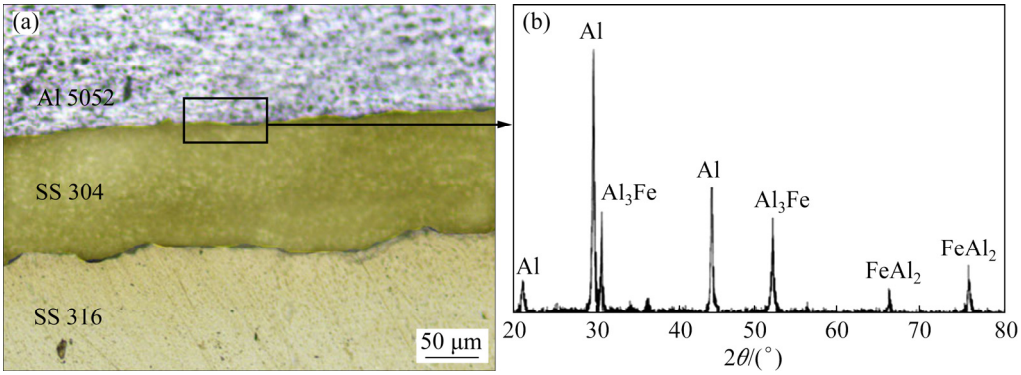

Fig. 11 Microstructure (a) XRD pattern (b) of Al 5052−SS 304−SS 316 interlayered explosive clad

presence of molten layer and the higher strength of stainless steel interlayer contribute to the enhancement of mechanical properties.

4.2.3 Copper interlayer

The use of a third alloy, other than flyer or base plate alloy, pure copper as interlayer, also exhibits an analogous positioning in the Al−steel biaxial welding window (Fig. 12(b)). On contrary to the aluminum and stainless steel interlayered cladding microstructure, both dissimilar clad interfaces display straight and wavy natured interfaces, along with a slender presence of molten layer. The first collision condition (flyer−interlayer) falls on the successful cladding regime and results in a wavy morphology, irrespective of the kinetic energy conditions. However, the copper−SS 316 collision condition (interlayer−base) falls well below the lower boundary and also displays a smooth interface with a non-uniform presence of straight and wavy natured interface.

The interface microstructure shows a wavy interface at both interfaces (Figs. 12(a, b)). However, there is a significant disparity between the two microstructures. The Al−Cu interface displays interfacial amplitude of 25 μm, while the Cu−steel interface measures to be 20 μm, for a higher kinetic energy condition (2.03 MJ/m^2). The wavy interface is attributed to the higher ductility, thermal conductivity (385 W/(m·K)) and thermal diffusivity (1.15 × 10^{-4} m^2/s) of copper interlayer. Copper conducts the generated heat 20 times faster than the stainless steel and supports the formation of the molten layer, visible as a dark patch (Figs. 12(a, c)). In lower kinetic energy conditions, molten layer formation is witnessed at the second interface, owing to the reduced collision velocity (Eq. (3)) and higher density of copper (8900 kg/m^3). Formation of molten layer at the dissimilar interface is similar to the findings of KUMAR et al [33]. It is inferred that thickness of the molten layer depends on the nature and properties of the interlayer. However, the thickness of the molten layer is more negligible than that of the interlayer-less clad. Hence, the use of metal/alloy having higher strength, ductility and better thermal properties pushes the lower boundary of the welding window, thereby enhancing the successful welding regime.

The experimental conditions for explosive clads with three different interlayers are superimposed on the Al 5052−SS 316 explosive cladding biaxial welding window (Fig. 13(a)). It is concluded that the use of interlayer relocates the lower boundary downwards and thereby enhances the welding regime by 40%. The extended lower boundary (Fig. 12) provides wider scope for industrial applications, estimated by

$$\beta = 0.3\sqrt{\frac{H_V}{\rho V_{w1}^2}} \tag{9}$$

4.3 Triaxial welding window

While biaxial welding window demonstrates the interaction between any two operational parameters such as collision velocity, V_w, and dynamic bend angle, β, the triaxial welding domain considers an additional operational parameter which provides further insight and better understanding of the collision conditions. The lower boundary and the extended lower boundary of the aluminum−stainless steel explosive clad with operational parameters of dynamic bend angle, β, flyer plate velocity, V_p, and collision velocity, V_w, as ordinates are developed (Fig. 13(b)) and the other boundaries are hidden.

The triaxial welding window disseminates the complicated interdependence prevailing among the

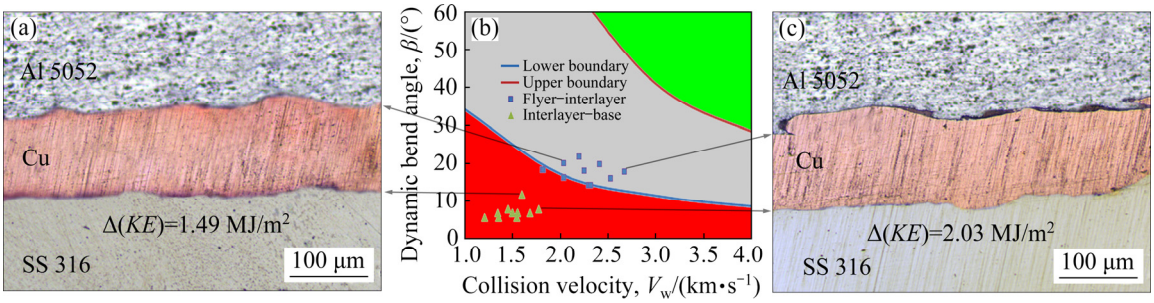

Fig. 12 Effect of Cu interlayer on microstructures (a, c) and biaxial welding window (b) of Al 5052−SS 316 explosive clad

three chosen operational parameters, and is appropriate for devising experimental conditions. Hence, it is concluded that the use of interlayer having higher density enhances the welding regime and interfacial characteristics. The formation of molten layer holds an adverse effect on the mechanical properties of the clad (presented in the next section).

4.4 Mechanical properties

4.4.1 Hardness variation

The Vickers microhardness profiles across various interlayered explosive clads are presented in Fig. 14. It is observed that the hardness values of the interlayered clads at the closer proximity of the interfaces are higher than those of the pre-cladded alloys and the clad without interlayer, respectively. The enhancement in hardness in closer proximity is consistent with the earlier study [23]. The increase in hardness is attributed to the dynamic collision and the subsequent interface hardening, local plastic deformation and the presence of stronger Al_3Fe and $FeAl_2$ compounds, as discussed in the previous section. Of the three different interlayered clads, the highest hardness is obtained while employing stainless steel and copper as interlayers due to the slender presence of molten region and the increased kinetic energy utilization. There is no significant

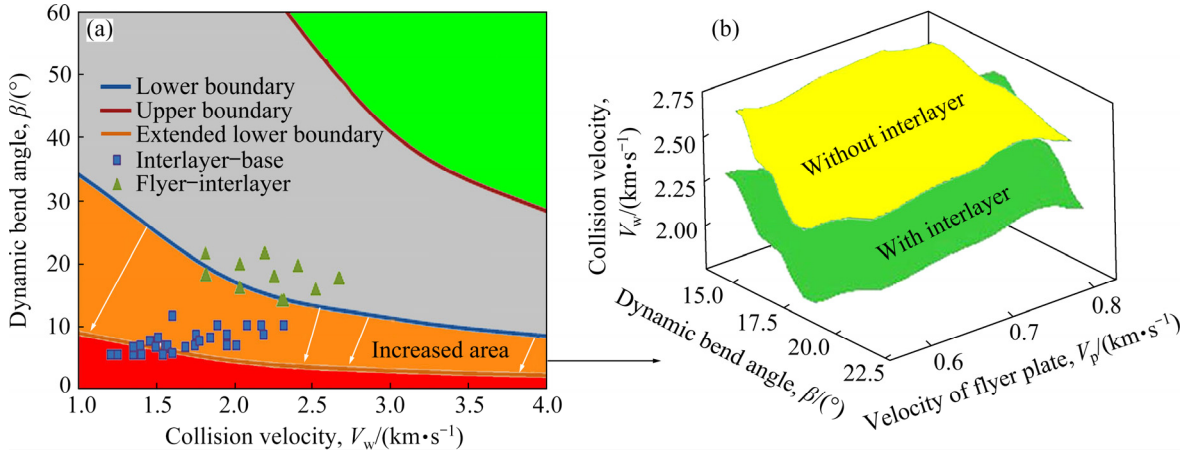

Fig. 13 Biaxial (a) and triaxial (b) welding windows for Al 5052−SS 316 explosive clad

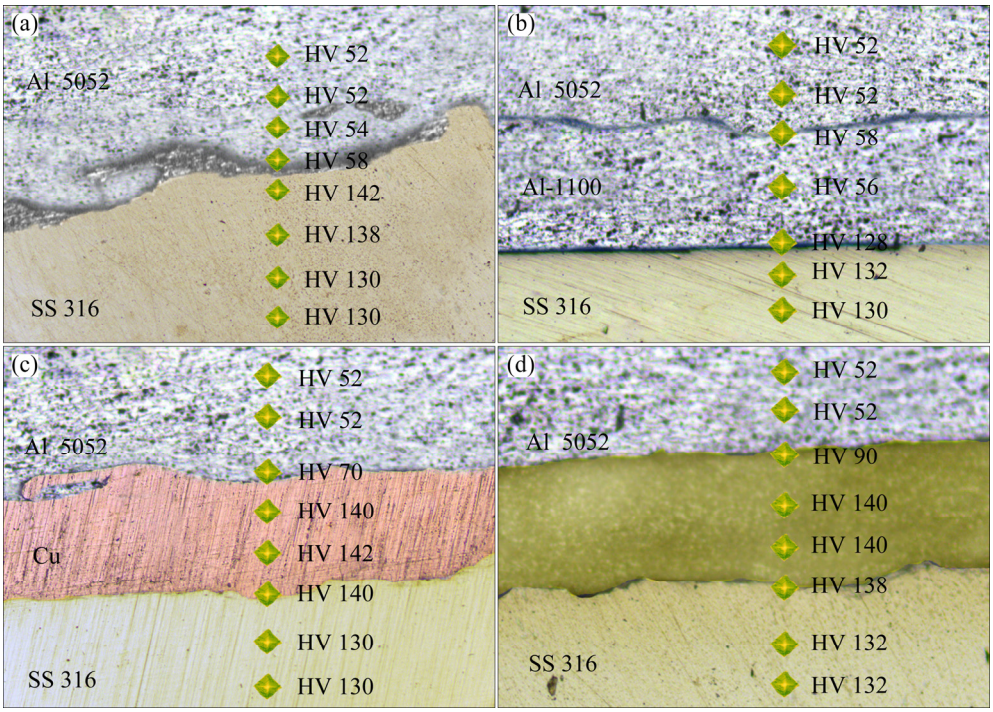

Fig. 14 Vickers microhardness variation across various interlayered explosive clads: (a) No interlayer; (b) Al 1100; (c) Pure copper; (d) SS 304

variation in hardness in the regions 2 mm apart from the interface due to the reduced plastic deformation experienced by the plates.

4.4.2 Ram tensile and shear strength

The ram tensile strength of various interlayered Al−SS explosive clads ranges from 230 to 290 MPa, while the shear strength varies from 143 to 202 MPa, depending on the nature of interlayer, operational parameters and interface microstructure (Fig. 15). Further, the maximum ram tensile and shear strengths are obtained for the stainless steel interlaced explosive clads at a standoff distance of 10 mm, an explosive mass ratio of 1.0 and an initial angle of 10°, which are 290 and 202 MPa, respectively. For the similar experimental condition the mechanical strength is about 6% lower (ram tensile strength: 273 MPa; shear strength: 184 MPa) for copper interlayered clads, owing to the properties of interlayer and intermetallic compound formation (details in the previous section). The aluminum interlaced dissimilar explosive clad provides the maximum ram tensile strength of 263 MPa and shear strength of and 180 MPa. The experimental setting prevailing on the periphery of the lower boundary results in higher mechanical strength. The minimum ram tensile and shear strengths of the interlayered clads are superior to the traditional clads (Al 5052−SS 316: 225 MPa) and weaker base alloy (aluminum: 180 MPa) as stated by ELANGO et al [34].

The fracture surface of the stainless steel interlaced dissimilar explosive clad (Fig. 16) reveals elongated dimples with few tear ridges at

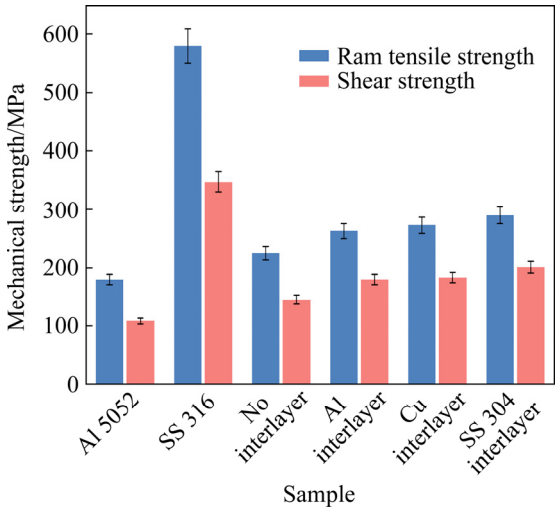

Fig. 15 Mechanical strength (peak values) of explosive clads with different interlayers

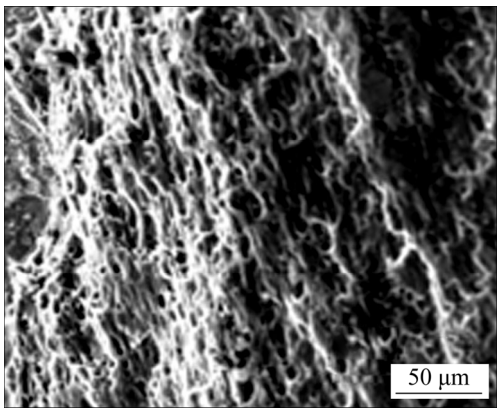

Fig. 16 Fracture surface of Al 5052−SS 304−SS 316 explosive clad

various locations to result in enhanced mechanical strength as reported by earlier researchers [35,36]. The fracture surface is free from cleavage or intergranular nature which characterizes brittle fracture mode.

5 Conclusions

(1) The use of interlayer suppresses the molten layer formation and promotes a strong Al−stainless steel explosive clad.

(2) Though the experimental conditions for interlayer explosive cladding prevail outside the biaxial welding window, metallurgically strong clads are obtained.

(3) The application of higher density metal/alloy as interlayer enhances the welding domain by shifting the lower boundary downwards.

(4) The maximum mechanical strength is obtained for stainless steel interlayered clads.

References

[1] THREADGILL P L, LEONARD A J, SHERCLIFF H R, WITHERS P J. Friction stir welding of aluminium alloys [J]. International Materials Reviews, 2009, 54(2): 49−93.

[2] DERAZKOLA H A, KHODABAKHSHI F. Intermetallic compounds (IMCs) formation during dissimilar friction-stir welding of AA5005 aluminum alloy to St-52 steel: Numerical modeling and experimental study [J]. The International Journal of Advanced Manufacturing Technology, 2019, 100(9): 2401−2422.

[3] SARAVANAN S, RAGHUKANDAN K. Thermal kinetics in explosive cladding of dissimilar metals [J]. Science and Technology of Welding and Joining, 2012, 17(2): 99−103.

[4] MURUGAN S P, CHEEPU M, NAM D G, PARK Y D. Weldability and fracture behaviour of low carbon steel/aluminium/stainless steel clad sheet with resistance spot

welding [J]. Transactions of the Indian Institute of Metals, 2017, 70(3): 759−768.

[5] MANESH H D. Assessment of surface bonding strength in Al clad steel strip using electrical resistivity and peeling tests [J]. Materials Science and Technology, 2006, 22(6): 634−640.

[6] DEQING W, ZIYUAN S, RUOBIN Q. Cladding of stainless steel on aluminum and carbon steel by interlayer diffusion bonding [J]. Scripta Materialia, 2007, 56(5): 369−372.

[7] HADDADI F, ABU-FARHA F. Microstructural and mechanical performance of aluminium to steel high power ultrasonic spot welding [J]. Journal of Materials Processing Technology, 2015, 225: 262−274.

[8] WANG H, QIN G L, GENG P H, MA X F. Interfacial microstructures and mechanical properties of friction welded Al/steel dissimilar joints [J]. Journal of Manufacturing Processes, 2020, 49: 18−25.

[9] YANG M, MA H H, SHEN Z W, CHEN Z W, DENG Y X. Microstructure and mechanical properties of Al−Fe meshing bonding interfaces manufactured by explosive welding [J]. Transactions of Nonferrous Metals Society of China, 2019, 29(4): 680−691.

[10] ACARER M, DEMIR B. An investigation of mechanical and metallurgical properties of explosive welded aluminum–dual phase steel [J]. Materials Letters, 2008, 62(25): 4158−4160.

[11] CARVALHO G H, GALVÃO I, MENDES R, LEAL R M, LOUREIRO A. Explosive welding of aluminium to stainless steel [J]. Journal of Materials Processing Technology, 2018, 262: 340−349.

[12] BECKER N, GAUTHIER D, VIDAL E E. Fatigue properties of steel to aluminum transition joints produced by explosion welding [J]. International Journal of Fatigue, 2020, 139: 105736.

[13] HAN J H, AHN J P, SHIN M C. Effect of interlayer thickness on shear deformation behavior of AA5083 aluminum alloy/SS41 steel plates manufactured by explosive welding [J]. Journal of Materials Science, 2003, 38(1): 13−18.

[14] CHEN X, INAO D, TANAKA S, MORI A, LI X, HOKAMOTO K. Explosive welding of Al alloys and high strength duplex stainless steel by controlling energetic conditions [J]. Journal of Manufacturing Processes, 2020, 58: 1318−1333.

[15] KUMAR C W D, SARAVANAN S, RAGHUKANDAN K. Influence of grooved base plate on microstructure and mechanical strength of aluminum–stainless steel explosive cladding [J]. Transactions of the Indian Institute of Metals, 2019, 72(12): 3269−3276.

[16] RIBEIRO J B, MENDES R, LOUREIRO A. Review of the weldability window concept and equations for explosive welding [J]. Journal of Physics: Conference Series, 2014, 500: 052038.

[17] CROSSLAND B. Explosive welding of metals and its applications [M]. Oxford: Oxford University Press, 1982.

[18] FINDIK F. Recent developments in explosive welding [J]. Materials & Design, 2011, 32(3): 1081−1093.

[19] MOUSAVI S A, SARTANGI P F. Experimental investigation of explosive welding of cp-titanium/AISI 304 stainless steel [J]. Materials & Design, 2009, 30(3): 459−468.

[20] SHI C G, YANG X, GE Y H, YOU J, HOU H B. Lower limit law of welding windows for explosive welding of dissimilar metals [J]. Journal of Iron and Steel Research International, 2017, 24(8): 852−857.

[21] SATYANARAYAN, MORI A, NISHI M, HOKAMOTO K. Underwater shock wave weldability window for Sn−Cu plates [J]. Journal of Materials Processing Technology, 2019, 267: 152−158.

[22] ÉMURLAEVA Y Y, BATAEV I A, ZHOU Q, LAZURENKO D V, IVANOV I V, RIABINKINA P A, TANAKA S, CHEN P. Welding window: Comparison of Deribas' and Wittman's approaches and SPH simulation results [J]. Metals, 2019, 9(12): 1323.

[23] SARAVANAN S, INOKAWA H, TOMOSHIGE R, RAGHUKANDAN K. Microstructural characterization of silicon carbide reinforced dissimilar grade aluminium explosive clads [J]. Defence Technology, 2020, 16(3): 689−694.

[24] SARAVANAN S, RAGHUKANDAN K, HOKAMOTO K. Improved microstructure and mechanical properties of dissimilar explosive cladding by means of interlayer technique [J]. Archives of Civil and Mechanical Engineering, 2016, 16: 563−568.

[25] SOMASUNDARAM S, KRISHNAMURTHY R, KAZUYUKI H. Effect of process parameters on microstructural and mechanical properties of Ti−SS 304L explosive cladding [J]. Journal of Central South University, 2017, 24(6): 1245−1251.

[26] MAHMOOD Y, CHEN P W, BATAEV I A, GAO X. Experimental and numerical investigations of interface properties of Ti_6Al_4V/CP-Ti/copper composite plate prepared by explosive welding [J]. Defence Technology, 2021, 17: 1592−1601.

[27] SARAVANAN S, RAGHUKANDAN K, KUMAR P. Effect of wire mesh interlayer in explosive cladding of dissimilar grade aluminum plates [J]. Journal of Central South University, 2019, 26(3): 604−611.

[28] SHIRAN M K, KHALAJ G, POURALIAKBAR H, JANDAGHI M, BAKHTIARI H, SHIRAZI M. Effects of heat treatment on the intermetallic compounds and mechanical properties of the stainless steel 321–aluminum 1230 explosive-welding interface [J]. International Journal of Minerals, Metallurgy, and Materials, 2017, 24(11): 1267−1277.

[29] MANIKANDAN P, HOKAMOTO K, FUJITA M, RAGHUKANDAN K, TOMOSHIGE R. Control of energetic conditions by employing interlayer of different thickness for explosive welding of titanium/304 stainless steel [J]. Journal of Materials Processing Technology, 2008, 195(1−3): 232−240.

[30] GRIGNON F, BENSON D, VECCHIO K S, MEYERS M A. Explosive welding of aluminum to aluminum: Analysis, computations and experiments [J]. International Journal of Impact Engineering, 2004, 30(10): 1333−1351.

[31] CARVALHO G H, GALVÃO I, MENDES R, LEAL R M, LOUREIRO A. Microstructure and mechanical behaviour of aluminium−carbon steel and aluminium−stainless steel clads produced with an aluminium interlayer [J]. Materials Characterization, 2019, 155: 109819.

[32] MENDES R, RIBEIRO J B, LOUREIRO A. Effect of explosive characteristics on the explosive welding of stainless steel to carbon steel in cylindrical configuration [J]. Materials & Design, 2013, 51: 182−192.
[33] KUMAR C W D, SARAVANAN S, RAGHUKANDAN K. Numerical and experimental investigation on aluminum 6061−V-grooved stainless steel 304 explosive cladding [J]. Defence Technology, 2020, 16: 1−12.
[34] ELANGO E, SARAVANAN S, RAGHUKANDAN K. Experimental and numerical studies on aluminum−stainless steel explosive cladding [J]. Journal of Central South University, 2020, 27(6): 1742−1753.
[35] ARGESI F B, SHAMSIPUR A, MIRSALEHI S E. Preparation of bimetallic nano-composite by dissimilar friction stir welding of copper to aluminum alloy [J]. Transactions of Nonferrous Metals Society of China, 2021, 31(5): 1363−1380.
[36] ROBIN L G, RAGHUKANDAN K, SARAVANAN S. Studies on wire-mesh and silicon carbide particle reinforcements in explosive cladding of Al 1100−Al 5052 sheets [J]. Journal of Manufacturing Processes, 2020, 56: 887−897.

不同夹层爆炸复合铝−不锈钢板的显微组织、强度和焊接窗口

S. SARAVANAN[1], K. RAGHUKANDAN[2]

1. Department of Mechanical Engineering, Annamalai University, Annamalainagar, 608002, Tamilnadu, India;
2. Department of Manufacturing Engineering, Annamalai University, Annamalainagar, 608002, Tamilnadu, India

摘　要：以 1100 铝、纯铜和 304 不锈钢为夹层，用爆炸复合法制备 5052 铝−316 不锈钢(Al 5052−SS 316)复合板。采用不同工艺参数，包括相隔距离、炸药质量比(炸药质量与飞片质量比)和倾斜角得到实验结果。夹层的使用使焊接窗口的下边界发生位移，焊接区域增大 40%。 在此基础上，设计考虑第三个操作参数影响的三轴焊接窗口。使用夹层后，传统 Al 5052−SS 316 炸药复合界面形成的连续熔融层转变为光滑的界面，其中没有或存在少量的金属间化合物。含夹层复合层的显微硬度、抗拉强度和剪切强度均高于传统爆炸复合层，且使用不锈钢夹层的 Al 5052−SS 316 爆炸复合层具有最高的显微硬度、抗拉强度和剪切强度。

关键词：显微组织；强度；焊接窗口；Al 5052；316 不锈钢；爆炸复合；夹层

(Edited by Wei-ping CHEN)